Bonding and interface states of Si:HfO_2 and Si:ZrO_2 interfaces

P. W. Peacock, K. Xiong, K. Tse, and J. Robertson*
Engineering Department, Cambridge University, Cambridge CB2 1PZ, United Kingdom
(Received 10 September 2005; revised manuscript received 10 January 2006; published 27 February 2006)

First principles calculations of the (100)Si:ZrO_2 and HfO_2 interfaces are presented. A number of interface configurations satisfying valence bonding requirements are constructed, and their total energies, relaxed structures, interface electronic states and band offsets are calculated. An interface with three coordinated oxygen sites is found to be the most stable oxygen-terminated interface for a 1×1 surface unit cell, and an interface with a tenfold coordinated Hf is the most stable for the metal-terminated interfaces. All the oxygen-terminated interfaces satisfying the valence requirements are found to be semiconducting, without gap states. The tenfold coordinated metal-terminated interface is found to be metallic, making this interface not useful for devices. The band offsets are found to vary by up to 0.7 eV for different interface terminations, showing that band offsets can in principle be controlled by chemistry.

DOI: 10.1103/PhysRevB.73.075328 PACS number(s): 77.55.+f, 73.20.−r, 68.55.−a, 85.40.−e

I. INTRODUCTION

The decrease of dimensions of complementary metal oxide silicon (CMOS) transistors has led to a need to replace their SiO_2 gate oxide with an oxide of higher dielectric constant (K), in order to maintain a small gate leakage current.[1,2] The oxide must satisfy various conditions such as be stable in contact with Si,[3] and have sufficient band offsets to be a barrier for both electrons and holes.[4] This restricts the choice to the oxides of Hf, Zr, La, Y, and Al, with the leading contenders being HfO_2, Hf silicates and their nitride alloys.[5–8] The oxides must also form a high quality interface with Si, with no interface states within the Si band gap. The current in the field effect transistor flows in the Si channel next to the interface, so the transistor performance depends fundamentally on the quality of this interface. However, despite the intensive work on high K oxides, the performance of devices with high K gates oxides is still worse than those with SiO_2 gate oxides, in terms of carrier mobility, charge trapping, and gate threshold voltages,[7–9] so that a deeper understanding of the interface is needed.

The first requirement of a possible interface structure is that it is insulating and it has no intrinsic interface states. Otherwise there will be no field effect. It turns out that this requirement depends fundamentally on the atomic coordinations and stoichiometry of the interface.[10] Thus the paper first considers the total energy and interface states of possible interface structures.

Another criterion for the choice of oxide is that the band offsets for both electrons and holes should be over 1 eV, to minimize leakage currents due to the injection of carriers into the oxide bands. Robertson[4] produced a simple analysis of the band offsets of many of the candidate oxides, based on the model of metal-induced gap states (MIGS), the charge neutrality level (CNL), and Schottky barrier pinning.[11] This proposed that the band offsets depended largely on alignment of the charge neutrality level in the bulk oxide and the Si via an interface dipole. Its predicted band offsets were in surprisingly good agreement with experimental values found subsequently. However, this model neglects the dependence of the interface dipole on the different termination[12] of oxide. These effects could be of order 1 eV, that is, as large as the Si gap. Thus, the second point of the paper is to understand how the band offsets vary with the termination (Hf or O) of the oxide layer.

A third point of interest is that many of the gate threshold problems which occur in high K oxide systems may arise from bonding defects at the oxide interfaces. Note that there are two interfaces, the bottom interface between the Si channel and the oxide, the "top" or "back" interface between the oxide and the gate electrode, which is presently doped polycrystalline Si. Sizeable shifts in the DC transistor gate threshold voltages have been attributed to interface defects at this back interface.[13,14] It is therefore necessary to be able to define an ideal interface in terms of its bonding, before we can define an interface defect. The ideal interface can be defined in terms of an abrupt interface with only Si-O and/or metal-O bonds. The possible defects are metal-Si bonds, vacancies, and antisites. The effect of such defects is described in Sec. VIII. Of course, a real interface may also have an interfacial layer of silicon dioxide present.

We represent the various interfaces here by periodic slab models of abrupt, crystalline, epitaxial interfaces. There has been considerable study of epitaxial oxides on Si[15–22] and by modeling.[10,23–31] However, the devices made by industry generally feature amorphous or nanocrystalline oxides with a narrow SiO_2 interfacial layer between the Si channel and the high K oxide. Nevertheless, our idealized models represent many of the problems involved.

II. CALCULATIONAL METHOD

Models of various interface structures are constructed as periodic supercells of Si and the oxide. Supercells with two interfaces and no vacuum and supercells with one interface and a vacuum layer are both used. The total energies of these supercells are calculated by the *ab initio* pseudopotential method and the density functional theory (DFT) using the CASTEP code.[32] The atoms are represented by Vanderbilt[33] ultrasoft pseudopotentials. The exchange correlation energy

 ©2006 The American Physical Society

TABLE I. Total energies of different phases of HfO_2, compared to cubic, per formula unit, for a plane-wave cutoff energy of 400 eV.

Phase	Energy (eV)
Cubic	0
Tetragonal	−0.09
Monoclinic	−0.20
Quartzlike	+2.1

is found from the Perdew-Wang PW91 version of the generalized gradient approximation (GGA) of DFT. We use a plane-wave cutoff energy of 350 eV and the forces are converged to 0.05 eV/Å. Some test calculations were carried out at 500 eV cutoff.

We modeled the interfaces by supercells containing two interfaces and no vacuum, about 27–45 Å perpendicular to the interface and 3.7 or 5.4 Å parallel to the interface, containing typically 25 to 47 atoms, 9-13 layers of Si, and 6–9 units HfO_2 or ZrO_2. All atomic positions including the cell lengths were allowed to relax, except that the supercell angles were all constrained to be 90°. Runs with both constrained and unconstrained symmetry were used. A number of runs were carried out with larger cell sizes parallel to the interface (but shorter perpendicular to the interface because of computer limits) in order to check for interface reconstructions. Indeed, interfaces with the "wrong" bonding do reconstruct across the interface. In a few cases, we also used cells with a vacuum layer. In this case, the Si slab is terminated by monohydride groups and dimerized Si, while the oxide slab is terminated by OH groups oriented normal to the interface. The OH group would prefer to be canted, but this lowers symmetry and increases the complexity of the relaxation, so we fixed the OH group positions in this case.

The total energies were calculated with typically six symmetrized *k* points on a Monkhorst-Pack grid. The density of states plots used typically a $12\times12\times3$ point grid.

The primary variable determining interface energetics, density of states, and band offsets is the local bonding. This condition holds whether the oxide is crystalline, amorphous or has some lattice mismatch. For example, HfO_2 exists in cubic, tetragonal, and monoclinic phases, which all have the same ionic bonding and are structurally closely related. The lower symmetry monoclinic phase is the most stable, as shown in Table I, and is usually found in experimental gate oxides. However, the cubic phase is simplest to treat both computationally and for structural models. But the conclusions hold for the other phases, because the key requirement is valence satisfaction, which holds for all phases. Once the basic interface is understood, the effects of lattice mismatch, disorder or defects can be added. Note that atomic displacements perpendicular to the interface can start to induce a tetragonal-like distortion in the bulk oxide away from the interface. The distortion is seen in the mean electrostatic potential, as described later. This effect is minimized by designing supercells so that the distortion from the top and bottom interfaces oppose one another. Then the distortion decays into the oxide. Another way to stop this is to freeze the plane of oxygen atoms at the supercell center.

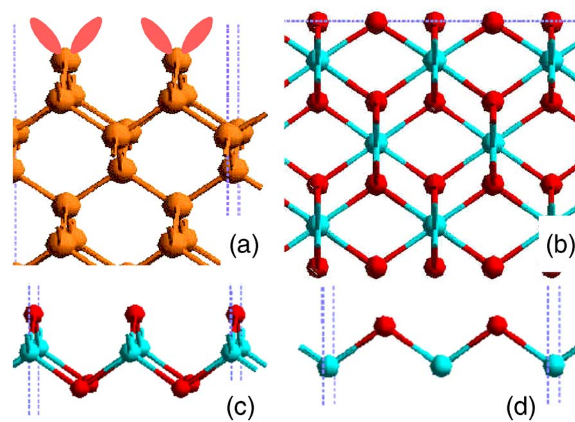

FIG. 1. (Color online) (a) Unreconstructed (100) surface of Si, (b) ideal (100) surface of HfO_2, (c) OHfO unit with nonpolar faces, (d) HfO unit with Hf-terminated face.

The lattice mismatch between Si and oxide does affect the energetics and band offsets. This effect is reduced as the supercell is able to relax perpendicular to the interface, so that the oxide and Si conserve their cell volume, the largest effect on energies and band gaps. Systematic effects on interface energies are minimized by using supercells with similar numbers of Si and oxide cells. For band offsets, the effect on the band gap was studied.

III. BONDING

The interface of Si and HfO_2 differs from the $Si:SiO_2$ interface because HfO_2 has ionic bonding, and also because Si and HfO_2 have no common element. Thus, while the $Si:SiO_2$ system consists of only Si-Si and Si-O bonds, the $Si:HfO_2$ interface can have Si-Si, Si-O, Hf-O, and Si-Hf bonds present.

HfO_2 and ZrO_2 exist in three phases, cubic fluorite, tetragonal, and monoclinic. The monoclinic (*m*) phase is the most stable, and most gate films consist of *m*-HfO_2. Nevertheless, the cubic HfO_2 lattice is interesting because it has the same tetrahedral symmetry as Si. The lattice constants of Si and cubic HfO_2 are 5.43 and 5.12 Å, respectively. HfO_2 is almost lattice matched to Si, so that an interface can be constructed so that the lattice of Si continues into the HfO_2, with the tetrahedral coordination of Si continuing onto the O site. In this respect, it resembles the $Si:NiSi_2$ and $Si:CaF_2$ interfaces.[34–36] This "cube on cube" epitaxy is expressed as $HfO_2(100)\parallel Si(100)$ and $HfO_2[001]\parallel Si[001]$. The lattice constant of cubic ZrO_2 is 5.07 Å. The cube on cube epitaxy has been achieved for *Y*-stabilized ZrO_2 and CeO_2 on Si.[16–18] The basic behavior of HfO_2 and ZrO_2 interfaces is similar.

First consider the bonding rules for the interface.[10] The ideal Si(100) surface is shown in Fig. 1(a). Atoms on the ideal Si(100) surface each have two dangling bonds per atom, each containing one electron. Thus, an ideal Si(100) surface would have half-filled gap states and be metallic.

The (100) and (111) surfaces of cubic HfO_2 are polar, being fully oxygen terminated as shown in Fig. 1(b). Nevertheless, nonpolar surfaces can be constructed by removing

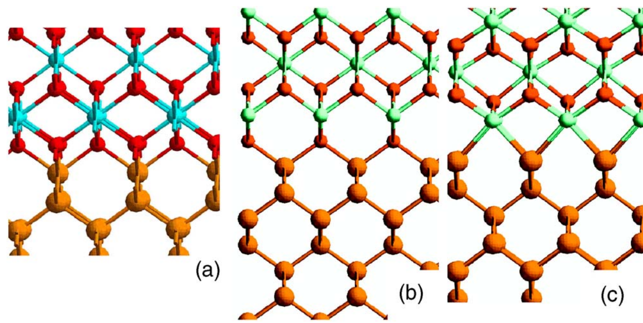

FIG. 2. (Color online) (100)Si:HfO_2 interfaces. (a) With O monolayer termination, (b) with $\frac{1}{2}$ O monolayer termination, and (c) with Hf-termination.

half a monolayer of oxygen atoms from each layer.[37] This allows us to construct a layer unit of HfO_2 with nonpolar faces on both sides, as shown in Fig. 1(c). On the other hand, we can create a HfO unit which is polar and Hf-terminated on one side, as in Fig. 1(d).

From this, we can construct (100) interfaces of HfO_2 having three different stoichiometries—polar and double O-terminated, nonpolar and single O-terminated, or polar and Hf-terminated, depending on if the O coverage at the interface is 1, $\frac{1}{2}$, or 0 monolayers. These are shown in Fig. 2.

We first consider the interface between Si(100) of Fig. 1(a) and the nonpolar face of HfO_2 of Fig. 1(c). This has a half monolayer of O at the interface, as in Fig. 2(b). The Si(100) surface has its two half-filled dangling bonds per atom, as in Fig. 1(a). The nonpolar face of HfO_2 however, has a closed shell, so this configuration leaves the two Si dangling bonds on the Si surface unpassivated, and the interface will be metallic. This is not desirable for devices.

On the other hand, we can add an O atom between each pair of Si's to form Si-O-Si bridges on the surface. This converts all the Si dangling bonds into Si-O bonds, and this face is now insulating. We now add the nonpolar face of HfO_2 to give the fully O-terminated interface shown in Fig. 2(a). This has the full O monolayer at the interface. Both individual components are insulating, so the total interface is insulating.

In the third case, an Hf-terminated unit of HfO_2, as in Fig. 1(d), has two unsatisfied Hf valences. This could make two covalent bonds per site. The ideal Si(100) surface also has two dangling bonds per site. Thus the Hf-terminated HfO_2 interface can form the required number of Hf-Si bonds to Si. Therefore we can add the Hf-terminated polar HfO unit to the Si(100) to create a passivated surface, as shown in Fig. 2(c).

In summary, for the symmetric interfaces, the nonpolar half monolayer O-covered HfO_2 face will make a metallic interface with Si(100), whereas the polar full monolayer O-covered face and the polar Hf-terminated face of HfO_2 each make an insulating interface.[10,28]

The real abrupt interfaces are more complex than these simple models, first because the high symmetry interfaces can relax, and second because there are a number of possible lower symmetry interfaces. These were found in tests of a wide range of supercells with large size parallel to the interface.

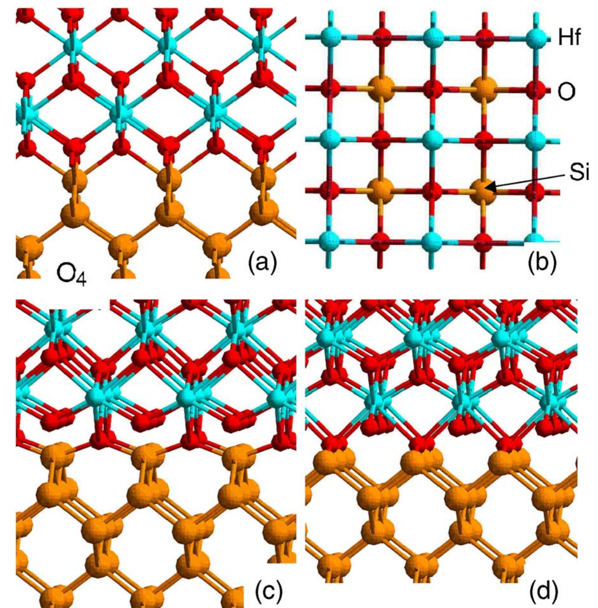

FIG. 3. (Color online) O_4 interfaces. (a) Ideal interface, (b) top view, (c), (d) side views of the relaxed interfaces.

Figure 3(a) shows again the ideal double-O terminated (100) interface. We call this the O_4 interface because the interfacial O's are initially fourfold coordinated. To minimize its energy, this interface relaxes to the structure shown in Figs. 3(c) and 3(d) from the [110] and $[\bar{1}10]$ directions. One oxygen has moved down to form a Si-O-Si bridge, and the other O has moved up into the HfO_2 layer. The interface has partially separated. The O in the Si-O-Si has tried to regain its divalence. The Si-O bond length is 1.93 Å, the Hf-O distance is 2.58 Å compared to a bulk value of 2.2 Å. At the upper O, the Hf-O distance is 2.05 Å. Figure 3(b) shows a view from above, along [001]. The final Hf atom lies in the face center of the four interface O's. The different vertical displacements of two oxygen sites decay into the oxide away from the interface.

Figures 4(a) and 4(b) shows a lower symmetry interface after relaxation called O_3 in which the oxygens are threefold coordinated. Although lower symmetry, it still fits in the small interface cell. There are two distinct oxygen sites, each lying in a (110) plane. Site O1 sits at the bridge site between two Si's and below an Hf ion. The second O lies above a Si and bonding to two Hf's. This interface is called O_3 because of the terminal O's have a planar threefold coordination. Site O1 has bond lengths of 1.89 Å for Si-O and 2.19 Å for Hf-O. Site O2 has bond lengths of 1.76 and 2.04 Å for Si-O and Hf-O. Figure 4(c) shows a top view, along [001], to compare with the O_4 interface in Fig. 3(c). The final Hf lies at an edge centre of two interface O's; the HfO_2 lattice has been displaced by $\frac{1}{2}a$ from that in O_4. The different vertical displacements of O1 and O2 sites decay away from the interface.

Figures 4(d) and 4(e) shows a still lower symmetry version of the O_3 interface, which we call O_{3T}. The terminal O's are again threefold coordinated. Now the HfO_2 lattice has been displaced by $\frac{1}{4}a$ compared to O_4 and the terminal O's

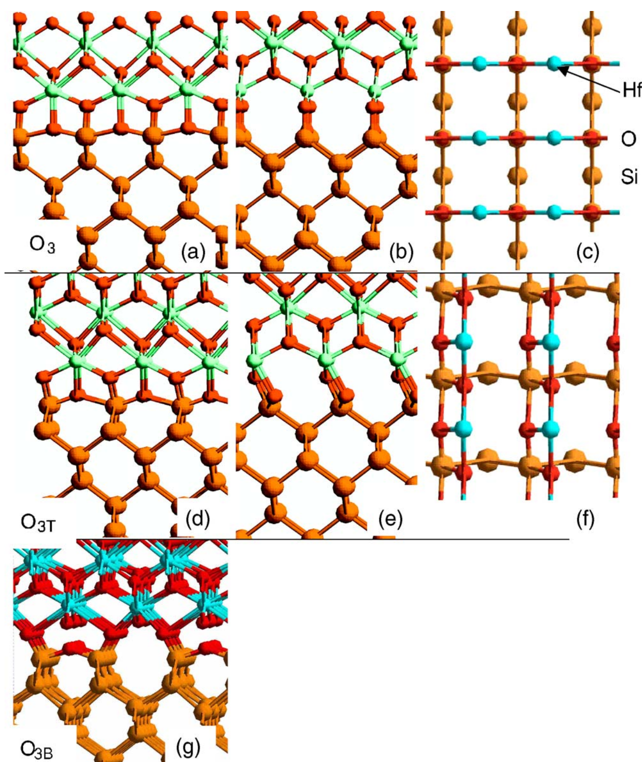

FIG. 4. (Color online) Various O_3 interfaces. (a), (b) Side views of the O_3 interface, (c) top view of O_3. (d), (e) Side views of the O_{3T} interface showing the offset of the Si and HfO_2 lattices, (f) top view of O_{3T}. (g) Side view of the O_{3B} interface. Note that absence of $\frac{1}{2}$ of the oxygens hanging below the first Hf layer.

lie in a nonplanar, threefold coordination. This is seen in the top view, shown in Fig. 4(f). This relaxed interface has the lowest energy. The oxygen coordination in both these O_3 interfaces resembles that in $HfSiO_4$.

Figure 4(g) shows another interface which can be built on the Si-O-Si bridge terminated 2×1Si(100) face. The terminal Si atoms now have a single dangling bond, and this can be bonded to oxygens which are threefold coordinated. To satisfy the valences in the first HfO_2 unit, half of the oxygens at the other O site must be absent.[27] We call this interface O_{3B}. This has the larger lateral supercell. The 2×1 cell is used here, a $2\times 2c$ was first used in Ref. 27

Some O-rich interfaces with more covalent bonding can be constructed. The simplest is to extend the Si lattice upwards by Si-O-Hf bridges, as if the bonding is in SiO_2. This forms the O_2 type interface shown in Fig. 5(a). The Si-O-Hf bridges are covalently bonded, and the O is divalent. The bonding switches to ionic on the other side of the Hf layer. We call this interface O_{2B}. Figures 5(a) and 5(b) show views of this interface from the [110] and $[\bar{1}10]$ directions. The quartz configuration of HfO_2 is about 2 eV unstable per formula unit compared to fluorite HfO_2 (Table I), so this interface is not very stable.

It turns out that the O_{2B} interface is relatively unstable because the high packing density of its oxygens needed by the interface is incompatible with the natural low density of a low coordination structure like bulk quartzlike HfO_2. On the other hand, if the surface Si's are allowed to dimerize and

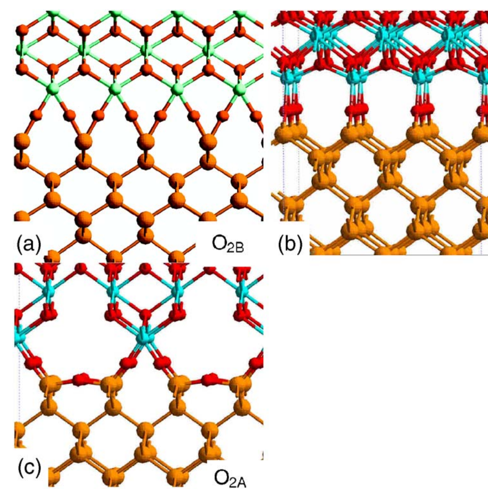

FIG. 5. (Color online) (a), (b) Side views of the O_{2B} interface, with the surface Si atoms having two Si-O-Hf bridges. (c) O_{2A} interface, with only one Si-O-Hf bridge per surface Si.

form lateral Si-O-Si bridges, this leaves one Si dangling bond per site. This face will form a half-density O_2 interface. We call this interface O_{2A} and it is shown in Fig. 5(c). Both 2×1 and centered (2×2) variants are possible. This would be the interface grown by atomic layer deposition (ALD) from molecular precursors.[38–40] It turns out that this interface actually has a low energy, because its low density is compatible with the O_2 coordination.

The O_4 interface with only a $\frac{1}{2}$ monolayer of oxygens, denoted O_{4V}, is metallic in its ideal configuration, Figs. 2(b) and 6(a), because it does not satisfy valence requirements. Its Fermi level would lie in the Si conduction band. If this interface is allowed to relax, then a distortion breaks Si-O bonds and forms the configuration seen in Fig. 6(b) for a centered 2×2 cell, leaving negatively charged dangling bonds. This then allows E_F to lie in a minimum of the density of states. Various versions of this reconstruction occur in larger cells. There are other similar configurations[26,29,30] which also do not form insulating interfaces.

We now consider the metal-terminated interfaces. The ideal Hf terminated interface was shown in Fig. 2(c). Figures 7(a) and 7(b) show views of this relaxed interface viewed

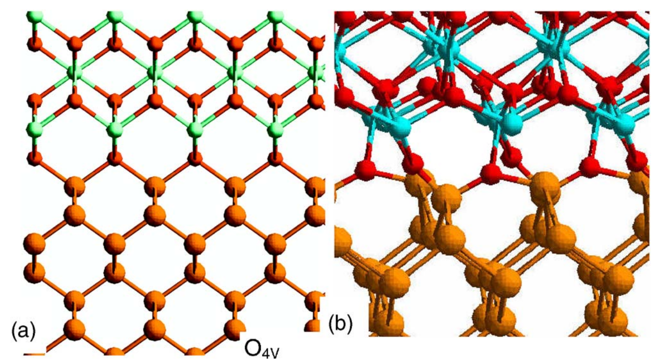

FIG. 6. (Color online) (a) Ideal O-terminated O_{4V} interface, with $\frac{1}{2}$ monolayer of oxygen. This is metallic. (b) Reconstructed O_{4V} interface, with broken Si-O bonds.

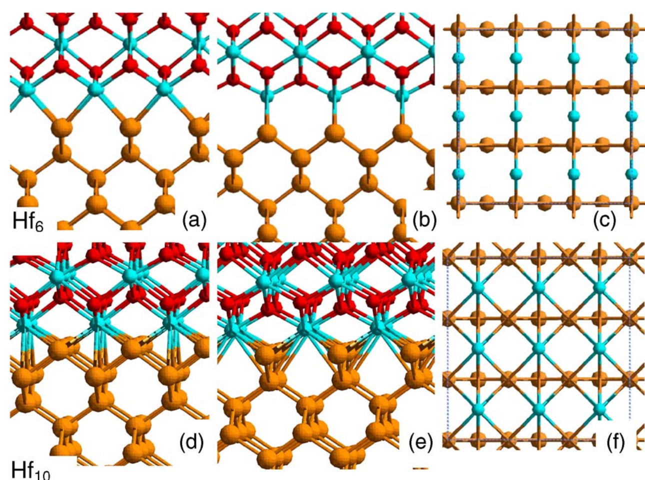

FIG. 7. (Color online) (a), (b) Side views of the relaxed 1×1 Hf_6 interface. (c), (d) Side views of the relaxed Hf_{10} interface. (e) Top view of Hf_{10}.

from [110] and [$\bar{1}$10] directions, and Fig. 7(c) shows a top view. The interface Hf ion is sixfold coordinated to two Si and four O atoms, so this is called the Hf_6 interface. This geometry conserves the tetrahedral coordinations of Si and O across the interface [equivalent to conserving the Si coordination across the (100)Si:NiSi$_2$ interface].[34] The Hf-Si bond length is 2.71 Å. It turns out that this is not the most stable Hf-terminated interface. The Hf can lower its energy by displacing the HfO$_2$ layer $\frac{1}{2}a$ along [110], so the Hf lies centrally in a hollow between the upper Si atoms. The Hf ion bonds to all the top four Si's (2.91 Å) and also to two Si on the next layer down (3.26 Å). Including the four O's in the HfO$_2$ layer, this Hf is now bonded to ten sites, so we call it the Hf_{10} interface. Figures 7(d) and 7(e) show views of the relaxed Hf_{10} interface from the [110] and [$\bar{1}$10] directions. Seen above in Fig. 7(f), the Hf atom lies in the same place above the top Si layer as in the O_4 interface, except that the interfacial O's are missing.

We note that all of the interface structures (except for O_{3B}) which satisfy valence requirements fit in the smallest surface unit cell 3.7 Å square. We checked that large lateral cells did not allow more stable reconstructions. These only occur for cases such as O_4 which do not satisfy valence requirements. Indeed, this is how the bonding rules were found.[27] These interface structures can be generalized to the cases where the oxide is monoclinic or tetragonal.

IV. INTERFACE TOTAL ENERGIES

The interface energies were calculated for the relaxed structures of supercells. The supercells contain just Si, oxide and two interfaces, and no vacuum. The supercells can contain different numbers of Si, Zr(Hf) or O atoms as the interface stoichiometry varies. The interface formation energy (per interfacial Si atom) is therefore given by

$$E_{form}=\frac{E_{total}-[nE_{ZrO_2}+mE_{Si}+l\mu_O]}{2q},$$

where the 2 is for the two interfaces per cell, q is the number of interface Si atoms per cell, n is the number of ZrO$_2$ or

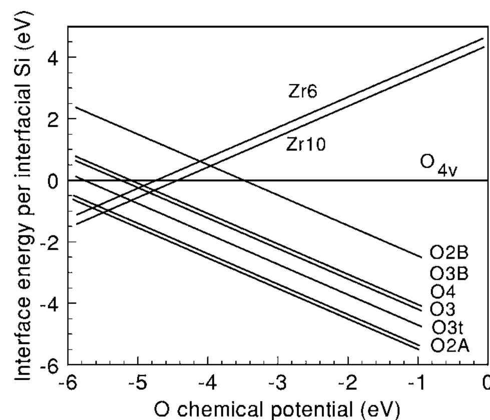

FIG. 8. Interface formation energies of various O- and Zr-terminated interfaces vs O chemical potential.

HfO$_2$ units in the cell, E_{ZrO_2} is the free energy of solid cubic ZrO$_2$ per ZrO$_2$ unit (or HfO$_2$), m the number of Si atoms in the cell, E_{Si} the free energy of solid Si per atom, l the number of excess oxygen atoms (not in a ZrO$_2$ or HfO$_2$ unit) and μ_O is the chemical potential of oxygen, a variable. Differences between the energies of HfO$_2$ and ZrO$_2$ were recently discussed by Gutowski *et al.*[41]

We are most interested in the relative stabilities of the different geometries, so we try to use supercells with similar numbers of Si and Zr(Hf) atoms in order to minimize any systematic errors. One such error is the strain energy arising from the in-plane lattice mismatch[26,31] between the Si and the oxide. Dong[31] considered both the relaxed and Si-clamped cases, we study the only relaxed case with a constant height of Si slab. In that case, the interfacial energy depends on the bonding mismatch. The effects of different oxide phases are of order 0.2 eV, and will be studied in detail elsewhere.

The formation energy per Si as a function of the O chemical potential is shown in Fig. 8 and in Table II. The energy of the O-rich interfaces such as O_4 decreases with increasing O chemical potential. The energy of the nonpolar interface O_{4V} is independent of the O chemical potential, and the energy of the Zr-rich interfaces increases with μ_O. We see that the O_{3T} interface is the most stable amongst the 1×1 O-rich interfaces by 0.3 eV, followed by O_3. Surprisingly, the most symmetric interface O_4 is not so stable. This is because at the O_3 interface, the interfacial oxygens bond across the interface to both Si and HfO$_2$ layers, whereas at O_4 they tend to bond either Si or Hf. The O_{2B} interface is 1.5 eV unstable, while we see that the O_{2A} interface is actually of comparable stability to O_{3T}, the most stable. We attribute the stability of O_{3T} to the similarity of the coordination and bond angles of O to those in HfSiO$_4$. The O_3 interface also has trivalent oxygens but the packing density is higher. The high stability of the O_{2A} interface could be due its low density at the interface, which takes up the lattice mismatch of Si and ZrO$_2$. Note that the O_{4V} interface is unstable and will tend to disproportionate into O-rich and Zr-rich interfaces, such as O_4 and Zr_{10}.

For the metal-rich interfaces, we see that the Zr_{10} interface is 0.3 eV more stable per interfacial Si than the Zr_6

TABLE II. Calculated total energies of different interface configurations of Si:ZrO_2 and Si:HfO_2, compared to the most stable for that stoichiometry.

Interface	Interface energy, per interface Si (eV)	
	ZrO_2	HfO_2
O_4	1.2	0.8
O_3	0.8	0.6
O_{3T}	0	0
O_{3B}	1.3	1.7
O_{2A}	−0.1	
M_6	0.3	0.3
M_{10}	0	0

interface. This arises from its higher Zr coordination. This difference is independent of any strain term, as the interfaces prefer the same strain.

The interface formation energies for the (100)Si:HfO_2 are similar to the ZrO_2 case. The ordering of stability for O_3, O_{3T}, O_{2A}, O_4, and O_{3B} is the same, there are differences in the values, as seen in Table II. The Hf_6 interface is again 0.3 eV per Si less stable than the Hf_{10} interface. The ordering of stabilities is similar to that found recently by Dong *et al.*[31] They also noted that the stabilities depended on the interface strain condition.

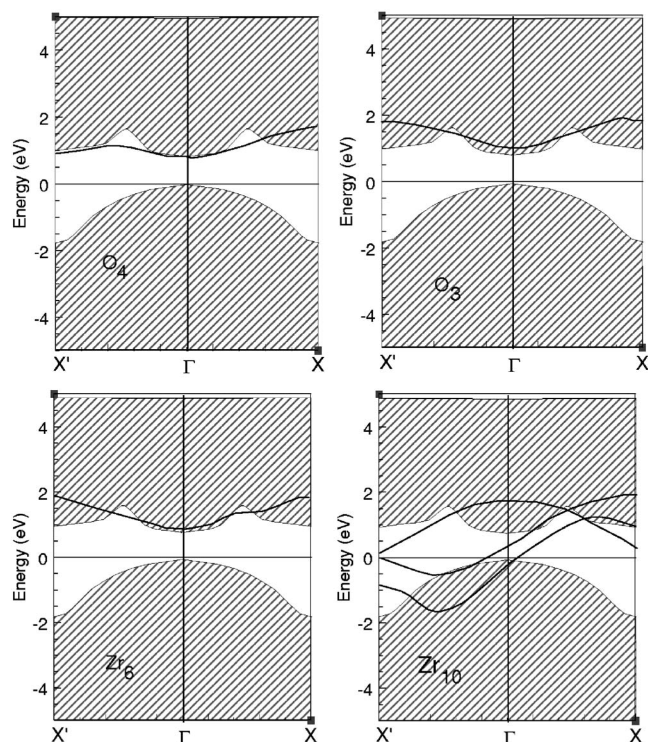

FIG. 9. Interface band structures of the O_4-, O_3-, Zr_6-, and Zr_{10}-terminated (100) interfaces, on the projected bulk band structure of Si. O_4, O_3, and Zr_6 are semiconducting, while Zr_{10} has bands crossing E_F and is metallic.

V. INTERFACE STATES

A field effect transistor requires the gate field to be able to sweep the Fermi level across the Si band gap to vary the carrier density. However, if there are interface states, the Fermi level will become pinned by them, and gate control is lost. Hence the interface between gate oxide and Si must possess no intrinsic interface states.

We have calculated the interface band structures of the various interface configurations, and plot this onto the bulk bands of Si projected onto (100), taken from Ihm *et al.*[42] The interface bands were calculated for a supercell with a single interface consisting of Si on ZrO_2 and a vacuum gap. The interface states are shown bold. Figure 9(a) shows the case of the O_4 interface. We see that the O_4 interface gives no interface states within the bulk Si band gap from 0 to 0.7 eV (in GGA). A similar result is found for the O_3 interface in Fig. 9(b) and the O_{2A} interface (not shown). These interfaces are all insulating, because they were constructed to satisfy valence requirements.

Figure 9(c) shows the interface band structure of the Zr_6 interface. We see that this also has no states within the Si gap from 0 to 0.7 eV. On the other hand, for the Zr_{10} interface in Fig. 9(d), three interface bands cross the gap. This band crossing causes the Zr_{10} interface to be metallic. This is a considerable difference to the Zr_6 interface. Thus, the Zr_6 interface would be suitable for field-effect transistors (FETs), but the Zr_{10} interface would not be. However, as the Zr_{10} (or Hf_{10}) is the more stable, in practice, it would be difficult to control the formation of this configuration. Hence we conclude that *only O-rich interfaces are suitable for FET devices*. Similar results are found for HfO_2 interfaces. The Hf_{10} interface is metallic, all the rest are insulating.

Gap states were found for the Zr_6 interface by Dong *et al.*,[31] in contrast to us. However, this could be because the valence band (VB) offset is the largest for this interface, comparable to the gap of ZrO_2 in GGA, so that accidentally the ZrO_2 conduction band lies energetically close to the Si VB. This makes it more difficult to tell the nature of the interface using the DOS method they used. It is clearer using a band plot.

Some interface configurations studied by Puthenkovilakam *et al.*[29] differ from ours. They chose some O-rich configurations which were metallic, with bands crossing E_F because they did not satisfy the valence requirements given earlier.[10] Those interfaces are not suitable. They were able to convert them into insulating interfaces by terminating unsatisfied valences with hydrogen atoms. However, this is not a realistic situation for real interfaces.

VI. DENSITY OF STATES AND BAND OFFSETS

The band offsets between Si and the oxide are key quantities in determining the oxide leakage performance. The conduction band (CB) offset is generally smaller than the VB offset, and so it is the more important parameter. The band offsets between the Si and oxide depend on any charge transfer across the interface. In the absence of charge transfer, the offset is given by the electron affinity rule. In the case of charge transfer, this occurs across the interfacial bonds.[11,12,43]

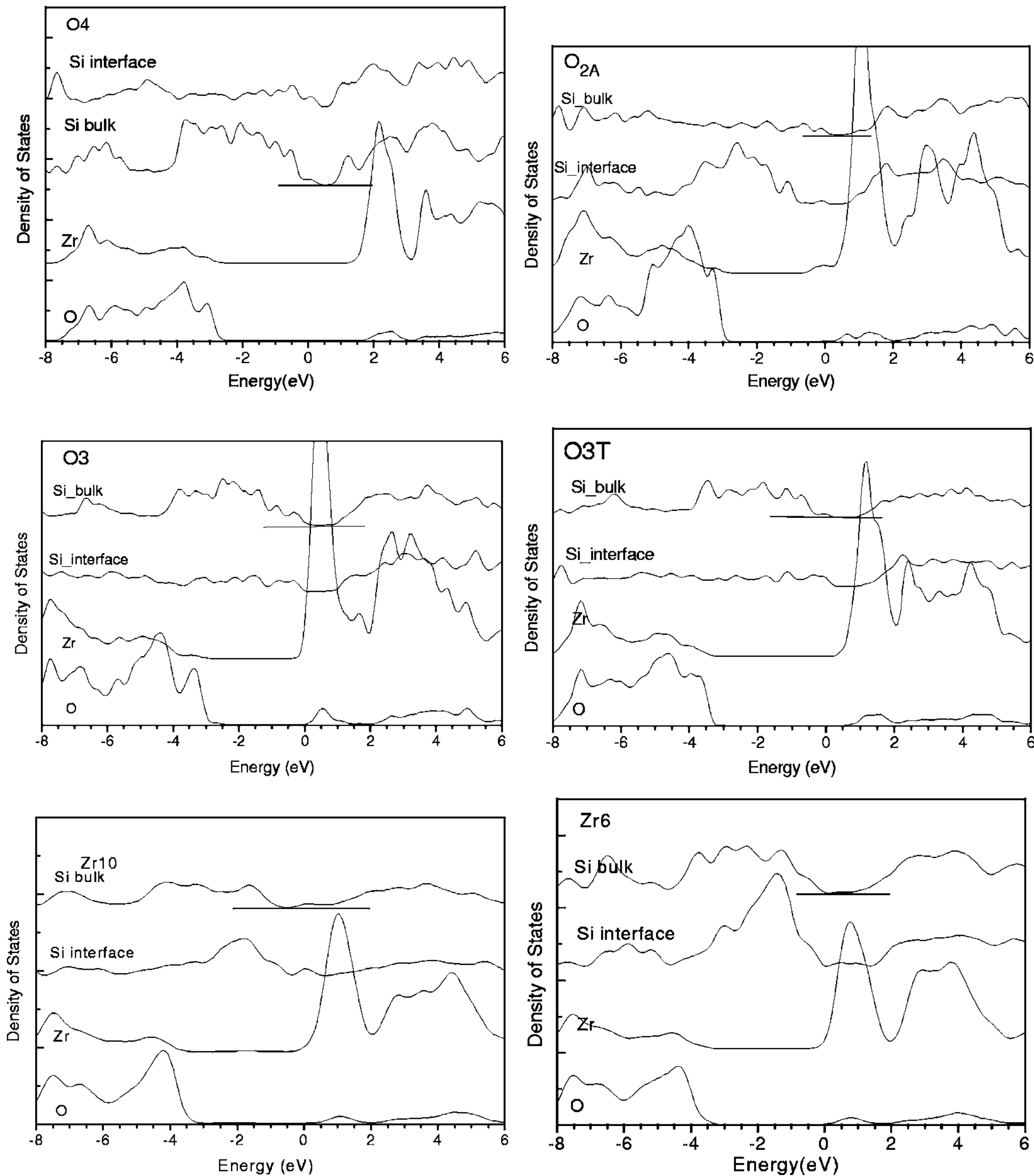

FIG. 10. Local density of states for interface and bulk sites of O_4, O_3, O_{3T}, O_{2A}, Zr_6, and Zr_{10} interfaces, from which the VB offsets are derived.

This will depend on the oxide termination at the interface.

The band offset is derived in our calculations by two methods. First, we calculate the local density of states (DOS) for atoms in the bulk Si and bulk HfO_2 or ZrO_2 in the supercell, as in Fig. 10, and find the energy shift between their valence band maxima. The calculated VB offsets using this method are given in Table III. The CB offsets are of greater interest, being smaller. The GGA is known to give the energies of occupied states accurately, but to give incorrect values for the empty states, tending to underestimate the band gap. Thus, to find the CB offsets, we take the calculated VB offset for each interface configuration and, using experimental values for the band gaps of Si and the ZrO_2 or HfO_2, we derive the CB offset.

A second method is to use the reference potential method.[44,45] The top of the valence band is found relative to the bulk average potential for pure Si and pure oxide. Then, the shift in average potential across the interface from Si to oxide is calculated for the supercell, for atoms far enough from the interface. This allows the difference in VB edges to be derived. This is analogous to the method used in photoemission using core levels.[46] An average potential is found by averaging the electrostatic potential perpendicular to the supercell axis Oz. Figure 11 shows a typical plot. Then the potential is averaged along Oz over one unit layer in the Si and in the oxide using a code that automatically locates the unit cells,[45] to give the average. Other authors[31] have corrected the band energies by a GW correction, we did not.

The two methods are complementary. The DOS method suffers because the interface DOS of the Si decays relatively slowly in bulk Si, so sufficient Si layers are needed. On the other hand, in the reference potential method, the poorer screening in the oxide means that the potential converges more slowly in the oxide.

TABLE III. Calculated VB offsets (eV) for (100)Si:ZrO_2 and Si:HfO_2, interfaces of different termination.

Interface	VB offset (eV)	
	ZrO_2	HfO_2
O_4	3.0	2.4
O_3	2.9	2.3
O_{3T}	3.3	2.6
O_{3B}	2.7	
O_{2A}	2.9	
Zr_6	3.3	3.25
Zr_{10}	2.4	2.2
Bulk CNL (GGA)	3.1	3.4

An important factor is the dependence of band energies on lattice constants. The oxides and Si lattices have a 5% mismatch, so the band offsets depend on the strain of the oxide as it expands to fit the Si lattice.[26,31]

The calculated VB offsets for (100)Si:ZrO_2 and Si:HfO_2 interfaces are given in Table III. We see that the offset is relatively constant for the various O-terminated interfaces. It does increase somewhat for O_{3T} so that the total variation is 0.4 eV. The values are quite close to that estimated earlier using the method of charge neutrality levels with GGA band structures (3.1 eV),[47] which neglects an explicit dependence of the dipole of the type of termination.[4] On the other hand, the VB offset varies quite strongly for the Zr-terminated case, from 2.4 eV for Zr_{10} to 3.3 eV for Zr_6. It is possible that 3.3 eV for Zr_6 is an underestimate. The VB offset in this case equals the ZrO_2 band gap of 3.4 eV in local density approximation. The Fermi level is forced into the ZrO_2 conduction band. But this is due to the underestimate of the oxide band gap in GGA. It is possible that when the gap is corrected, that the VB offset could be higher.

Our offsets are very similar to those of Dong *et al.*[31] for the Zr terminated interfaces, but show a smaller range of variation for the O-terminated cases. This shows that the termination has an important influence on the offset.

The variations can be analyzed in terms of the interface dipole. For the O-terminated interfaces, the interface dipole is Si^+-O^- which tends to raise energy levels on the oxygen side. The oxygen ions at the O-terminated interfaces have a similar ionic charge. The dipole can vary because of a different O-Si distance projected normal to the interface. Many of the O interfaces have two O sites. Overall, the average dipole is rather constant, except for O_{3T}, which has a longer projected O-Si distance. This accounts for the small range of VB offsets for O-terminated interfaces.

For the Zr-terminated interfaces, we find that the ionic charges on Si^- and Zr^+ ions are similar for both interfaces. However, the Si-Zr distance projected normal to the interface is shorter for the Zr_{10} than the Zr_6 interface (1.4 vs 2.2 Å), as the Zr sits in a hollow of the four Si's in Zr_{10}. Thus the dipole with its positive end in the oxide is larger for Zr_6, and this lowers the energies on the oxide side for Zr_6 compared to Zr_{10}, increasing the VB offset of Zr_6.

The band offsets for Si:HfO_2 interfaces are found to be similar. The VB offsets of O_4, O_3, and O_{3T} are found to be smaller than for ZrO_2 but in the same order. Those for Hf_6 and Hf_{10} are similar to those of ZrO_2.

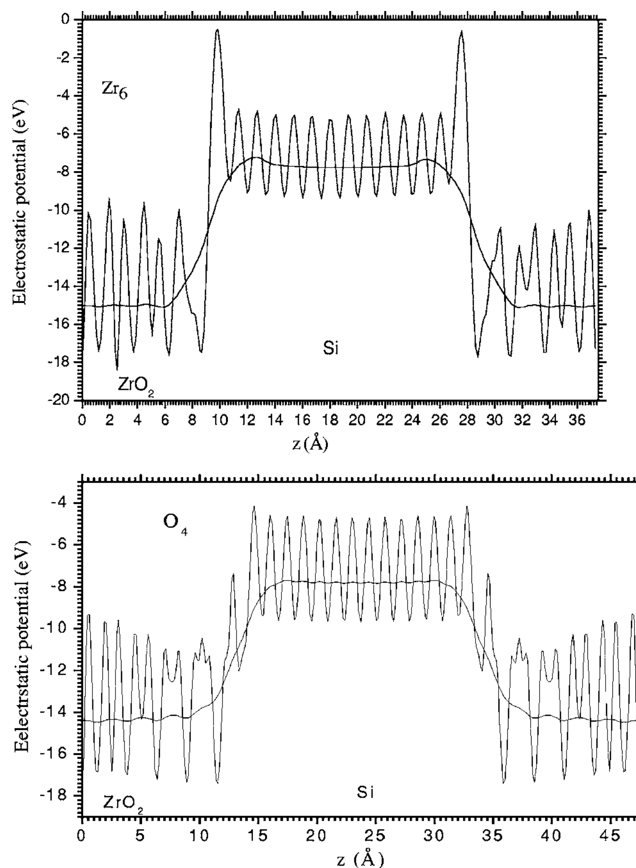

FIG. 11. Electrostatic potentials of supercells with Zr_6 and O_4 interfaces. The smoother line is the averaged potential.

An interesting aspect is that the large range of the VB offset between Zr_6 and Zr_{10} of 0.8 eV, which is a large fraction of band gap of Si. The Schottky barrier pinning factor S of ZrO_2 is 0.5 (Ref. 4). This pinning has raised the possibility that it may not be possible to vary the effective work functions of metals on ZrO_2 or HfO_2 by a sufficient range to create *n*- and *p*-type metal-oxide semiconductor gate metals.[48] The present results show that, in theory at least, the offset can be tuned over a large fraction of the Si band gap just by changing the interface termination, despite $S=0.5$. So it should also be possible for metals.

VII. COMPARISON WITH EXPERIMENT

A. Interface structure

There are few experimental cases of (100)ZrO_2 grown on (100)Si without any interfacial SiO_2 layer. One of these is the study of Wang and Ong.[17] Their TEM images suggest an interface structure similar to the O_4 structure, based on the alignment of the Si and Zr rows. The oxygens cannot be seen, due to their low atomic number. As O_4 is not the lowest energy interface, this suggests that the interface which forms experimentally in this case is determined by kinetics not energy, by the preferred location of the first arriving oxygen or

Zr atom. Simulations of growth from atomic precursors[49] show that the first monolayer of Zr occupies the center of the cube of the surface Si's on the unreconstructed 1×1 surface—the Zr_{10} site. This could then grow into a bulk ZrO_2 with a Zr_{10} interface. In reality, this silicide phase would be oxidized during the over-growth of ZrO_2 layers because of the relatively easy transport of additional oxygen through the oxide. It transforms the Zr_{10} sites to O_4 sites by replacing Zr-Si bonds by Zr-O-Si links. We speculate that the formation of Zr_{10} not only templates the start of (100) epitaxy, it also inhibits the (110)//(100) epitaxy which other cubic oxides are prone to show.[50,51] Thus, metal last terminations can help enforce (100) oxides on (100)Si as recently seen experimentally.[52]

Of course, in many cases, an interfacial layer of SiO_2 grows and it obscures any possible epitaxial relationship. Often, for device reasons, a thin interfacial SiO_2 layer is added intentionally, to improve the carrier mobility. On the other hand, in the Ge:HfO_2 system, GeO_2 is less stable than SiO_2, and so more evidence of epitaxial growth of ZrO_2 and HfO_2 on Ge is seen, even when prepared under standard ALD conditions.[53,54] This is despite the worse mismatch of Ge than Si to the oxide lattices, and mismatch dislocations are seen. These mismatch dislocations do not seem to alter the band offsets.

Most device oxides are grown by ALD. There have been a number of simulations of the ALD growth of HfO_2 on Si by ALD from $HfCl_4$ precursors.[38–40] The oxidant is water, so the Si starts from a hydroxyl terminated 2×1 surface, with lateral Si-O-Si bridges and single -OH groups attached to each surface Si. It turns out that there is no room to pack a monolayer of $HfCl_4$ or similar tetravalent molecular precursors on this (100)Si surface. Thus, the oxide naturally grows into the O_{2A} interface. This is another case of kinetic control.

B. Band offsets

There have been numerous measurements of the band offsets of ZrO_2 and HfO_2 on Si and Ge, due to the importance of this quantity.[55–65] There are two main methods, photoemission or internal photoemission. Photoemission studies the evolution of the valence band DOS and core levels of Si and oxide, with the overgrowth of the oxide layer on the Si. The offset of the valence band can be found using the core level reference method, or the offset of the valence band edges measured directly. The CB offset is then derived using the known band gaps. Alternatively internal photoemission measures the transitions from the Si valence band to the oxide conduction states. In this case, the Si gap is subtracted to give the CB offset.

For ZrO_2 on Si, Miyazaki[55] found a VB offset of 3.35 eV, Sayan[56] 3.4 eV, Wang[57] 2.95 eV, Rayner[58] 3.3 eV by photoemission, which converts to CB offsets of 1.3 to 1.75 eV for ZrO_2 with a 5.8 eV gap, the gap value from Wang.[57] These VB offsets are very similar to those calculated here for O-terminated interfaces. Afansiev[58] found a barrier of 3.1 eV by internal photoemission or a CB offset of 2.0 eV. This is slightly larger than found by photoemission.

For HfO_2, Sayan[60] found a VB offset of 3.28 to 3.44 eV [however, see their discussion (Ref. 61)], Oshima[62] 3.0 eV, Li *et al.*[63] 3.05–3.10 eV, and Renault[64] 2.95 eV, which convert to CB offsets of 1.4 to 1.8 eV for a 5.9 eV gap. Afanasev[65] found a barrier of 3.1 eV by internal photoemission, or a CB offset of 2.0 eV. The VB offsets from photoemission are again very similar to those calculated here for the O-terminated interfaces.

There have been no attempts to measure the change in offsets as a function of termination for ZrO_2 or HfO_2 or Si. However, Dong *et al.*[66] have studied the barrier height change of Ni on a ZrO_2 surface as a function of the surface oxygen deficiency. They found a 0.76 eV change. This is the order of magnitude to be expected for a change of termination of ZrO_2. It compares fairly well with the 0.6 eV change between the O_4 and Zr_{10} termination calculated here. Note that large shifts in offsets have been reported by Fulton[67] but these were attributed to dipoles across an SiO_2 layer. They are still not fully understood.

The various estimates of CB offset, both calculated and experimental, lie in the range 1.3 to 2.0 eV. The first, key conclusion is that they all exceed the necessary 1.0 eV needed to limit Schottky emission from the Si, and so the oxides fulfil their key requirement of maintaining a low leakage current.[4] Otherwise, the precise value is not so critical. The second conclusion from Table I is that it is possible in principle to vary the CB offset by chemical control of the interface, although this may be difficult in practice. Thus, there is not a single unique value of the CB offset for any oxide on Si. The third aspect is that the experimental and calculated values should give the correct chemical *trends*, for example whether the CB offsets increases from HfO_2 to Hf silicate to La_2O_3, in order that oxides are chosen correctly in terms of their "scalability."[68]

VIII. INTERFACE DEFECTS

The interface structures calculated in Sec. IV provide a basis to understand interface defects. In metal-oxide-semiconductor capacitors and FETs, there are shifts in the threshold voltages. Those varying with time are due to charge trapping, mainly at bulk O vacancies.[69,70] Other shifts are seen to vary with the thickness of the HfO_2 overlayer. Various checks on how the shifts vary with channel doping, Boron effects, gate electrode polarity, etc., led workers to attribute these shifts to a specific interaction between the HfO_2 and the top poly-Si gate electrode rather than with the channel.[13,71] The shifts are similar to a "pinning" of the Fermi level at the interface of the poly-Si, so that its work function did not vary by the full amount across its gap with doping. Further analysis suggested that the effect was not a general effect due to metal-induced gap states, but to specific Hf-Si bonds.[13,14]

The perfect Si:HfO_2 interface was *assumed* by Hobbs and Chau[13,14] to be a fully O-terminated interface, with only Hf-O bonds and no Hf-Si bonds. For this, one can introduce interfacial Hf-Si bonds in two ways, by creating O vacancies or by creating Si antisites on O sites.[70]

We noted that the O_4 and Hf_{10} interface have the same symmetry viewed from above, with the Hf ion lying above four Si's in both cases, Figs. 3(b) and 7(f). Removing inter-

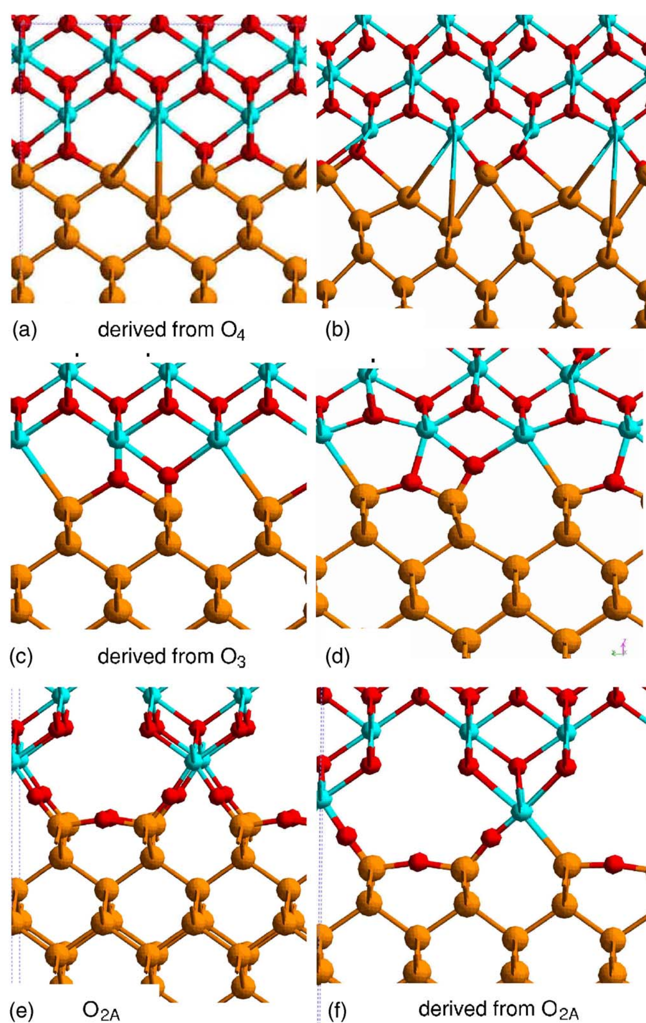

FIG. 12. (Color online) Some interface defect configurations. (a), (b) Unrelaxed and relaxed O divacancies at the O_4 interface. (c), (d) Unrelaxed and relaxed O divacancies at the O_3 interface. (e), (f) O_{2A} interface and monovacancy at the O_{2A} interface.

facial O's from O_4 to create O vacancies gives a continuous transition from the O_4 to Hf_{10} interfaces. However, we noted in Sec. III that a single interfacial O vacancy leads to a metallic situation, O_{4V}. This site is unstable to reconstruction. It is also unstable and it will tend to disproportionate into O_4 and Hf_{10}, according to the total energies in Fig. 9. Thus, for higher stability, we introduce interfacial O vacancies in *pairs*. The atoms across the vacancy then relax, to form one or more weak Hf-Si bonds. The O vacancy has a "negative *U*" of atoms (not electrons). Thus, there can be continuous transformation of O_4 to Hf_{10} by removing pairs of interfacial O atoms.

Figures 12(a) and 12(b) show the unrelaxed and relaxed interfaces with a pair of interface O vacancies. The structure has relaxed in Fig. 12(b) to form direct Hf-Si bonds across the vacancy site, two per vacancy. We have constructed supercells with different size lateral unit cells to simulate different concentrations of interface vacancies. The supercell length along Oz is reduced compared to those used for perfect interfaces in Sec. III, to keep the total number of atoms with reasonable limits for computing purposes. The local density of states has been calculated for this interface. The Hf-Si bonds are found to give rise to localized interface states lying within the Si gap. The state tends to lie at about 0.3 eV below the Si CB edge.

A similar procedure is possible for the O_3 interface. Two oxygens are removed each time. Figure 12(c) shows the unrelaxed interface, and Fig. 12(d) shows the relaxed interface with one Hf-Si bond per vacancy pair. The local density of states was calculated and the Hf-Si bond also gives rise to a gap state in the Si gap.

The O_{2A} interface has Hf-O-Si bridges with divalent O sites. This case is different. It is possible to remove O atoms singly. Each O vacancy creates one Hf-Si covalent bond after relaxation. These bonds have twice the bond order than those at the O4 interface. Nevertheless, the local density of states also shows that the Hf-Si bonds also create states in the Si gap.

The presence of gap states due to Hf-Si bonds inhibits the *n*- and *p*-type dopants in the poly-Si from shifting the Fermi level in the poly-Si all the way from CB to VB at the interface.[72] Thus, there is a restricted range of Fermi level shifting, which is called pinning. These results confirm that the formation of interfacial Hf-Si bonds is a likely cause of this pinning effect found experimentally in devices.[13] It has also been confirmed by calculations by Hobbs and Fonseca,[13] Pourtois,[73] and Gavartin.[74] Similar results are expected for defects at $Si:ZrO_2$ interfaces.

IX. CONCLUSIONS

We have carried out first principles calculations of the energetics and energy states of the $(100)Si:HfO_2$ and ZrO_2 interfaces. A number of interface configurations satisfying valence bonding requirements few found, and their total energies, relaxed structures, interface electronic states, and band offsets were calculated. An interface O_{3T} with three-coordinated oxygen sites is found to be the most stable oxygen-terminated interface for a 1×1 surface unit cell, and an interface with a tenfold coordinated Hf or Zr is the most stable for the metal-terminated interfaces. An interface with divalent O was found to be of similar high stability to O_{3T} for a 2×1 cell. All the oxygen-terminated interfaces which satisfy the valence requirements are found to be semiconducting, without interface gap states. The tenfold coordinated metal-terminated interface is found to be metallic, making this interface not useful for devices. However, this interface is proposed to be useful experimentally for templating epitaxial cube-on-cube growth on (100)Si. The band offsets are found to vary by up to 0.7 eV for different interface terminations, showing that band offsets could in principle be controlled by chemistry. The standard interface is fully oxygen-terminated. The presence of Hf-Si bonds across the interface introduces a gap state in the upper Si gap, and has the effect of pinning the Si Fermi level in the upper gap.

ACKNOWLEDGMENT

The authors are grateful to S. J. Clark for the use of his potential code.

*Electronic address: jr@eng.cam.ac.uk

[1] G. Wilk, R. M. Wallace, and J. M. Anthony, J. Appl. Phys. **89**, 5243 (2001).
[2] J. Robertson, Eur. Phys. J.: Appl. Phys. **28**, 265 (2004).
[3] H. J. Hubbard and D. G. Schlom, J. Mater. Res. **11**, 2757 (1996).
[4] J. Robertson, J. Vac. Sci. Technol. B **18**, 1785 (2000).
[5] M. Copel, M. Gribelyuk, and E. Gusev, Appl. Phys. Lett. **76**, 436 (2000).
[6] M. R. Visokay, J. J. Chambers, A. L. P. Rotondaro, A. Shanware, and L. Colombo, Appl. Phys. Lett. **80**, 3183 (2002).
[7] L. A. Ragnarsson, S. Guha, M. Copel, E. Cartier, N. A. Bojarczuk, and J. Karasinski, Appl. Phys. Lett. **78**, 4169 (2001).
[8] E. P. Gusev *et al.*, Tech. Dig. - Int. Electron Devices Meet. **2001**, 20.1.
[9] S. Datta, Tech. Dig. - Int. Electron Devices Meet. **2003**, 28.8.
[10] P. W. Peacock and J. Robertson, Phys. Rev. Lett. **92**, 057601 (2004).
[11] W. Mönch, Surf. Sci. **300**, 928 (1994).
[12] R. T. Tung, Mater. Sci. Eng., R. **35**, 1 (2001).
[13] C. C. Hobbs *et al.*, Technical Digest for VLSI Symposium (IEEE, Kyoto, 2003), p. 9; IEEE Trans. Electron Devices **51**, 971 (2004); **51**, 978 (2004).
[14] R. Chau *et al.*, Extended abstracts of International Workshop on Gate Insulators (IEEE, Tokyo, 2003), pp. 124–126.
[15] R. A. McKee, F. J. Walker, and M. F. Chisholm, Phys. Rev. Lett. **81**, 3014 (1998).
[16] S. J. Wang, C. K. Ong, S. Y. Xu, P. Chen, W. C. Tjiu, J. W. Chai, A. C. H. Huan, W. J. Yoo, J. S. Lim, W. Feng, and W. K. Choi, Appl. Phys. Lett. **78**, 1604 (2001).
[17] S. J. Wang and C. K. Ong, Appl. Phys. Lett. **80**, 2541 (2002).
[18] T. Ami *et al.*, Appl. Phys. Lett. **78**, 1361 (2001).
[19] S. Guha, N. A. Bojarczuk, and V. Narayanam, Appl. Phys. Lett. **80**, 766 (2002).
[20] A. Fissel, J. Dabrowski, and H. J. Osten, J. Appl. Phys. **91**, 8986 (2002).
[21] G. Apostolopoulos, G. Vellianitis, A. Dimoulas, M. Alexe, R. Scholz, M. Fanciulli, D. T. Dekadjevi, and C. Wiemer, Appl. Phys. Lett. **81**, 3549 (2002).
[22] D. O. Klenov, D. G. Schlom, H. Li, and S. Stemmer, Jpn. J. Appl. Phys., Part 2 **44**, L617 (2005).
[23] C. J. Forst, C. Ashman, K. Schwarz, and P. E. Blochl, Nature (London) **427**, 56 (2004).
[24] P. W. Peacock and J. Robertson, Appl. Phys. Lett. **83**, 5497 (2003).
[25] X. Zhang, A. A. Demkov, H. Li, X. Hu, Y. Wei, and J. Kulik, Phys. Rev. B **68**, 125323 (2003).
[26] V. Fiorentini and G. Gulleri, Phys. Rev. Lett. **89**, 266101 (2002).
[27] P. W. Peacock and J. Robertson, *Crystalline Oxides on Semiconductors*, MRS Symposia Proceeding No. 747 (Materials Research Society, Pittsburgh, 2002), p. 99.
[28] J. Robertson and P. W. Peacock, Phys. Status Solidi B **241**, 2236 (2004).
[29] R. Puthenkovilakam, E. A. Carter, and J. P. Chang, Phys. Rev. B **69**, 155329 (2004).
[30] R. Puthenkovilakam, E. A. Carter, and J. P. Chang, J. Appl. Phys. **96**, 2701 (2004).
[31] Y. F. Dong, Y. P. Feng, S. J. Wang, and A. C. H. Huan, Phys. Rev. B **72**, 045327 (2005).
[32] V. Milman, B. Winkler, J. A. White, C. J. Pickard, and M. C. Payne, Int. J. Quantum Chem. **77**, 895 (2000); M. D. Segall *et al.*, J. Phys.: Condens. Matter **14**, 2717 (2002).
[33] D. Vanderbilt, Phys. Rev. B **41**, R7892 (1990).
[34] D. Cherns, C. J. D. Hetherington, and C. J. Humphreys, Philos. Mag. A **49**, 165 (1984).
[35] D. R. Hamann, Phys. Rev. Lett. **60**, 313 (1988).
[36] R. M. Tromp and M. C. Reuter, Phys. Rev. Lett. **61**, 1756 (1988).
[37] A. Christensen and E. A. Carter, Phys. Rev. B **58**, 8050 (1998).
[38] L. R. C. Fonseca, A. A. Demkov, and A. A. Knizhnik, Phys. Status Solidi B **239**, 48 (2003).
[39] M. Deminsky *et al.*, Surf. Sci. **549**, 67 (2004).
[40] J. Garavin, L. Fonseca, G. Bersuker, and A. L. Shluger, Microelectron. Eng. **80**, 412 (2005).
[41] W. Zheng, K. H. Bowen, J. Li, L. Dabkowski and M. Gutowski, J. Phys. Chem. A **109**, 11521 (2005);J. E. Jaffe, R. A. Bachorz, and M. Gutowski, Phys. Rev. B **72**, 144107 (2005).
[42] J. Ihm, M. L. Cohen, and D. J. Chadi, Phys. Rev. B **21**, 4592 (1980).
[43] R. T. Tung, Phys. Rev. Lett. **84**, 6078 (2000).Phys. Rev. B **64**, 205310 (2001).
[44] A. Franciosi and C. G. Van de Walle, Surf. Sci. Rep. **25**, 1 (1996); C. G. Van de Walle and R. M. Martin, Phys. Rev. B **35**, 8154 (1987).
[45] H. M. Al-Allak and S. J. Clark, Phys. Rev. B **63**, 033311 (2001).
[46] E. A. Kraut, R. W. Grant, J. R. Waldrop, and S. P. Kowalczyk, Phys. Rev. Lett. **44**, 1620 (1980).
[47] P. W. Peacock and J. Robertson, J. Appl. Phys. **92**, 4712 (2002).
[48] Y. C. Yeo, T. J. King, and C. Hu, J. Appl. Phys. **92**, 7266 (2002); J. K. Schaeffer, C. Capasso, L. Fonseca, S. Samavedam, D. Gilmer, Y. Liang, O. Adetutu, C. Hobbs, E. Lckowski, R. Gregory, Z. X. Jiang, K. Moore, B. Y. Nguyen, D. Roan, B. E. White, and P. J. Tobin, Tech. Dig. - Int. Electron Devices Meet. **2004**, 287.
[49] C. J. Forst, P. E. Blochl, and K. Schwarz, Comput. Mater. Sci. **27**, 70 (2003).
[50] H. Nagata, T. Tsukahara, S. Gonda, M. Yoshimoto, and H. Koinuma, Jpn. J. Appl. Phys., Part 2 **30**, L1136 (1991).
[51] V. Naraynan, S. Guha, N. A. Bojarczuk, and F. M. Ross, J. Appl. Phys. **93**, 251 (2003).
[52] H. J. Osten *et al.* (unpublished).
[53] H. Kim, C. O. Chui, K. C. Saraswat, and P. C. McIntyre, Appl. Phys. Lett. **83**, 2647 (2003).
[54] E. P. Gusev, H. Shang, M. Copel, M. Gribelyuk, C. D'Emic, P. Kozlowski, and T. Zabel, Appl. Phys. Lett. **85**, 2334 (2004).
[55] S. Miyazaki, J. Vac. Sci. Technol. B **19**, 2212 (2001).
[56] S. Sayan *et al.*, Phys. Status Solidi B **241**, 2246 (2004).
[57] S. J. Wang, A. C. H. Huan, Y. L. Foo, J. W. Chai, J. S. Pan, Q. Li, Y. F. Dong, Y. P. Feng, and C. K. Ong, Appl. Phys. Lett. **85**, 4418 (2004).
[58] G. B. Rayner, D. Kang, Y. Zhang, and G. Lucovsky, J. Vac. Sci. Technol. B **20**, 1748 (2002).
[59] V. V. Afanasev, M. Houssa, A. Stesmans, and M. M. Heyns, Appl. Phys. Lett. **78**, 3073 (2001); J. Appl. Phys. **91**, 3079 (2002).
[60] S. Sayan, E. Garfunkel, and S. Suzer, Appl. Phys. Lett. **80**, 2135 (2002).
[61] S. Sayan *et al.*, J. Appl. Phys. **96**, 7485 (2004).
[62] M. Oshima, S. Toyoda, T. Okumura, J. Okabayashi, and H. Kumigashira, Appl. Phys. Lett. **83**, 2172 (2003).
[63] Q. Li, S. J. Wang, K. B. Li, A. C. H. Huan, J. W. Chai, J. S. Pan, and C. K. Ong, Appl. Phys. Lett. **85**, 6155 (2004).

[64] O. Reynault, N. T. Barrett, D. Samour, and S. Quiais-Marthon, Surf. Sci. **566**, 526 (2004).
[65] V. V. Afanasev, A. Stesmans, F. Chen, X. Shi, and S. A. Cambell, Appl. Phys. Lett. **81**, 1053 (2002).
[66] Y. F. Dong, S. J. Wang, J. W. Chai, Y. P. Feng, and A. C. H. Huan, Appl. Phys. Lett. **86**, 132103 (2005).
[67] C. C. Fulton and R. J. Nemanich, J. Appl. Phys. **96**, 2665 (2004).
[68] Y. C. Yeo, T. J. King, and C. Hu, IEEE Trans. Electron Devices **50**, 1027 (2003).
[69] A. Kerber, E. Cartier, L. Pantisano, R. Degraeve, T. Kauerauf, Y. Kim, G. Groeseneken, H. E. Maes, and U. Schwalke, IEEE Electron Device Lett. **24**, 87 (2003).
[70] K. Xiong, J. Robertson, M. C. Gibson, and S. J. Clark, Appl. Phys. Lett. **87**, 183505 (2005).
[71] E. Cartier, V. Narayanan, E. P. Gusev, P. Jamison, B. Linder, M. Steen, K. K. Chan, M. Frank, M. Copel, S. Zafar, C. Cabal, C. D. Emic, J. Newbury, S. Guha, and R. Jammy, Tech. Dig. VLSI Symp (IEEE, Hawaii, 2004) p. 44.
[72] K. Xiong, P. W. Peacock, and J. Robertson, Appl. Phys. Lett. **86**, 012904 (2005).
[73] G. Pourtois, L. Pantisano, T. Schram, and M. Heyns, Microelectron. Eng. **80**, 280 (2005).
[74] J. Gavartin, A. Shluger, and G. Bersuker, Proceeding: SEMATECH Workshop, Austin, TX, Sept 2005.